A mathematical model for sidelobe level optimization of variable inclination continuous transverse stub antenna

Kexin Wang[1] (iD), Xue Lei[2], Jun Gao[2], Tianpeng Li[2] and Mingyang Zhao[1]

[1]Institute of Information System Engineering, Information Engineering University, Zhengzhou, China and [2]National Digital Switching System Engineering and Technological R&D Center, Zhengzhou, China

CAMBRIDGE UNIVERSITY PRESS

Abstract

A mathematical model of variable inclination continuous transverse stub (VICTS) antenna for low sidelobe design is proposed in this paper. VICTS antenna is an antenna with continuous transverse stubs on the parallel-plate waveguide and additional branches attached to the transverse stubs to generate radiation. The antenna using this technique has high aperture efficiency and keeps a significant solution for high-gain antenna. However, the sidelobe level (SLL) of this antenna is relatively high and increases continuously as the pitch angle decreases. This paper presents a fast calculation model for the SLL of VICTS antennas using leaky-wave theory and antenna array theory. The full-wave simulation results and model calculation results are in good agreement, so this model can be used for SLL suppression of VICTS antennas in different frequency bands. By controlling the aperture field distribution to be tapered, the SLL is suppressed to -23.7 dB using this mathematical model.

Introduction

With the rapid advance of science and technology including satellite communication, mobile satellite communications that work at high frequencies such as Ku-band have been further studied [1–3]. In order to meet the application requirements of high-speed moving objects such as vehicles and airplanes, the antenna must have a low profile and aerodynamic shape. A typical parabolic antenna has the characteristics of high gain and low cross-polarization [4, 5]. Meanwhile, the volume of parabolic antenna keeps extremely bulky. The phased array antenna, which has fast electronic beam scanning capability and a low profile, usually cost too much due to a large number of expensive T/R components [6, 7].

Variable inclination continuous transverse stub (VICTS) antenna is a novel antenna evolved from continuous transverse stub (CTS) antenna [8–12]. It has the same low profile, high gain, and wide bandwidth as the CTS antenna. At the same time, the beam scanning capability has been significantly improved, which can be widely applied in various situations [13, 14]. The VICTS antenna consists of a radiation plate and a feeding plate placed in parallel, as shown in Fig. 1. The beam scanning can be realized by rotating the two plate of the VICTS antenna relatively, and the beam direction of the radiation pattern can be quickly calculated according to the relative rotation angle [15]. VICTS antenna is a very popular solution for mobile satellite communication due to its simple structure, easy processing, and low cost.

In previous work, some methods of suppressing the sidelobe level (SLL) have been applied to the CTS antenna. The ridge waveguide slot array (RWSA) is adopted as a linear source to feed the CTS array [16]. The RWSA was built to obtain low SLL of -25 dB by controlling the size and position of the slots. In [17], an antenna is composed of a 45° linear polarizer and 32-slots fed by a 1-to-256 power divider. The *E*-plane and *H*-plane of the antenna are rotated to positions that are 45° away from the two principal axes of the pattern. The SLL in *E*-plane is reduced to -28 dB. The SLL in *E*-plane of the CTS array fed by non-uniform corporate feed network can be suppressed to -28 dB by employing the Gaussian distribution of the slots [18]. In [19], the researchers propose a closed-form expression for VICTS antenna patterns with the same excitation amplitude for each element. Such an amplitude distribution cannot be realized in practice. But the mathematical model in this paper is based on the physical parameters of VICTS antenna and can be used in the actual antenna design.

As far as the author's knowledge and all open literature are concerned, there is no low SLL optimization method for VICTS antenna yet. Inevitably, the SLL deteriorates to -13.5 dB. This paper presents a calculation method for the pattern of VICTS antenna at different scanning angles. This method can be used to optimize the SLL of VICTS antenna. High consistency is obtained by comparing the results of theoretical calculation and full-wave simulation.
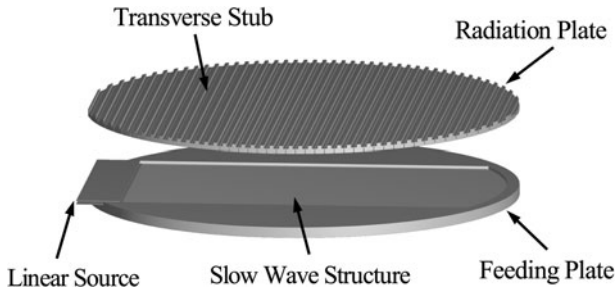
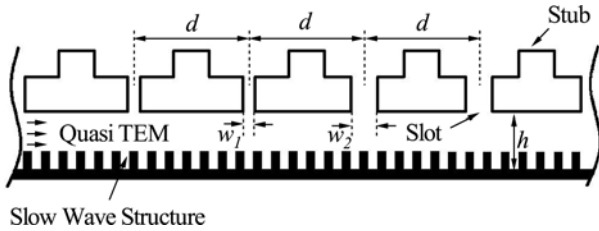**Fig. 1.** Main structure diagram of VICTS antenna.

Fig. 2. Partial side view of VICTS antenna.

Theoretical model of VICTS antenna

This section gives the main structure and the principles of the VICTS antenna. As shown in Fig. 2, the radiation plate is composed of several slot in series, which match the active impedance of the array through a single matching section [20]. In order to make the aperture field distribution relatively uniform, two types of radiation slots with the same period d and different widths w_1 and w_2 are selected.

The radiation efficiency of the slot is controlled by multiple parameters, which can be calculated by the full-wave simulation software CST [9]. The radiation efficiency of the slot increases as the height h decreases, and as the width $w_i(i = 1, 2)$ increases. When w_i and h are determined, the radiation efficiency of the slot is also determined and recorded as $\eta_{0i}(i = 1, 2)$.

In addition, the radiation efficiency of the slot is related to the operating frequency of the antenna. It is necessary to obtain the radiation capability of the slot through full-wave simulation while scaling to a different frequency.

Mathematical model of radiation pattern of VICTS

The theoretical model of the VICTS antenna is shown in Fig. 3 when there is no relative rotation between the radiation plate and feeding plate. Although the radiation plate keeps circular, the energy is mainly distributed in the rectangle which is slightly wider than the width of the parallel plate waveguide. Therefore, only the contribution in the rectangular region is considered in order to simplify the analysis. The length L_x and width L_y of the rectangle correspond to the narrow beamwidth axis and the wide beamwidth axis of the radiation pattern, respectively.

In the main radiation region, the number of narrow slots is N_1. The number of wide slots is N_2, thus

$$L_x = d(N_1 + N_2) \tag{1}$$

Since each slot is parallel to the feed port, the electric field at different positions of the same slot does not change with the change

of the Y coordinate. $\dot{I}_n$ can be expressed as follows:

$$\dot{I}_n = I_n \, e^{jk\varepsilon_e dn} \tag{2}$$

where $k = 2\pi f/c$, f is the operating frequency, c is the speed of light in vacuum, ε_e is the equivalent dielectric constant of the slow-wave structure [21, 22], I_n is the unit amplitude, which can be expressed as

$$I_n = \sqrt{\prod_{i=1}^{n} (1 - \eta_{i-1})\eta_i} \quad n = 1 \ldots N_1 + N_2$$

$$\eta_i = \begin{cases} 0, & i = 0 \\ \eta_{01}, & 0 < i \leq N_1 \\ \eta_{02}, & N_1 < i \leq N_1 + N_2 \end{cases} \tag{3}$$

In this case, one-dimensional linear array theory can be used to calculate the antenna's radiation pattern $F(\theta, \varphi)$.

$$F(\theta, \varphi) = \sum_{n=1}^{N_1+N_2} C\dot{I}_n e^{jkdn \sin\theta \cos\varphi} \tag{4}$$

where C is the cell pattern.

As shown in Fig. 4, when the two plates of the VICTS antenna rotate relatively, the angle between the radiation slot and the equal phase plane is denoted as γ. The amplitude and phase of different positions on the same slot are no longer the same, so the radiation pattern cannot be simply calculated as before.

The VICTS antenna is regarded as a two-dimensional array by dispersing the different positions on the radiation slot at equal distance. The element spacing in X-axis direction and Y-axis direction is d_x and d_y, respectively [19].

$$d_x = d/\cos\gamma \quad d_y = d/\sin\gamma \tag{5}$$

There are $M = a\lfloor L_y/d_y \rfloor$ rows in the Y-axis direction where a is a coefficient. The larger a is, the more points there are, and the more accurate the calculation results are, but the larger the amount of calculation is. a should be increased to ensure the accuracy when the rotation angle γ is larger. $\lfloor \bullet \rfloor$ is a down rounding function.

The number of elements in each row in X-axis direction is $N = \lfloor L_x/d_x \rfloor$, of which the small radiation capacity is N_0. Therefore, with the decrease of the Y coordinate, the number of narrow slots is N_0 increases step by step.

$$N_0 = \left\lfloor \frac{L_x - \tan\gamma\left(L_y - 2\frac{m-1}{a}d_y\right) - d_x}{2d_x} + 1 \right\rfloor$$
$$m = 1 \ldots M \tag{6}$$

The coordinates of each element can be expressed as follows:

$$X_{mn} = \left(n + \frac{m}{a} - \left\lfloor \frac{m}{a} \right\rfloor - 1\right)d_x$$
$$Y_{mn} = \frac{m}{a}d_y \tag{7}$$

When the radiation plate and the feeding plate rotate relatively, the electric field of each point is different because the radiation
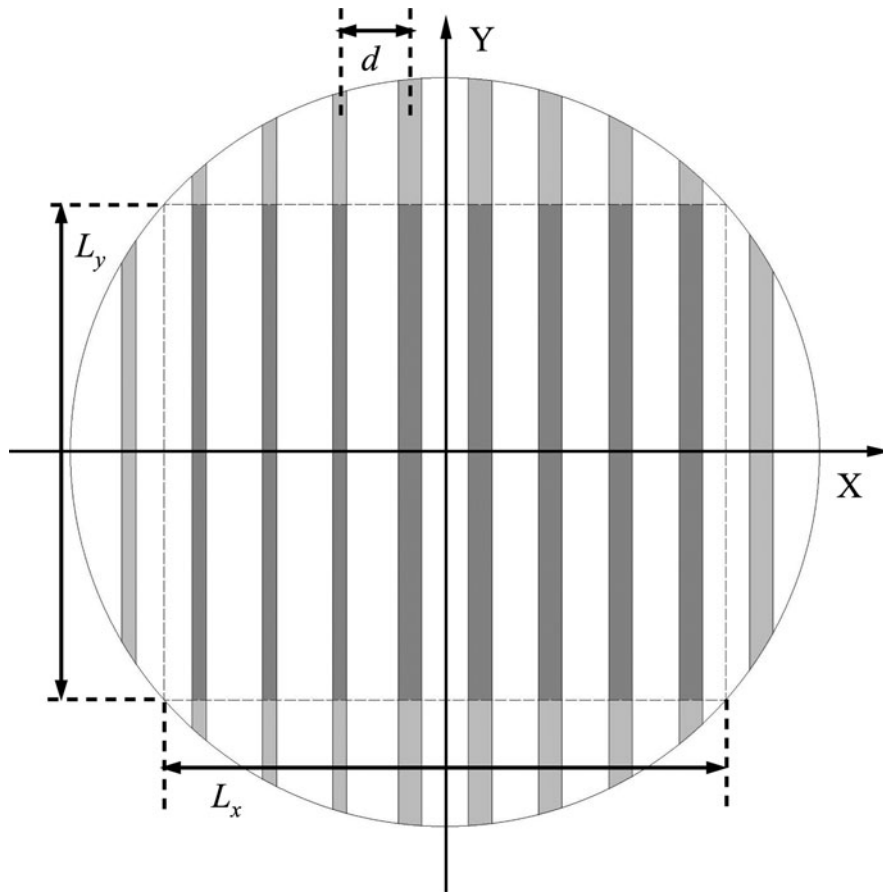
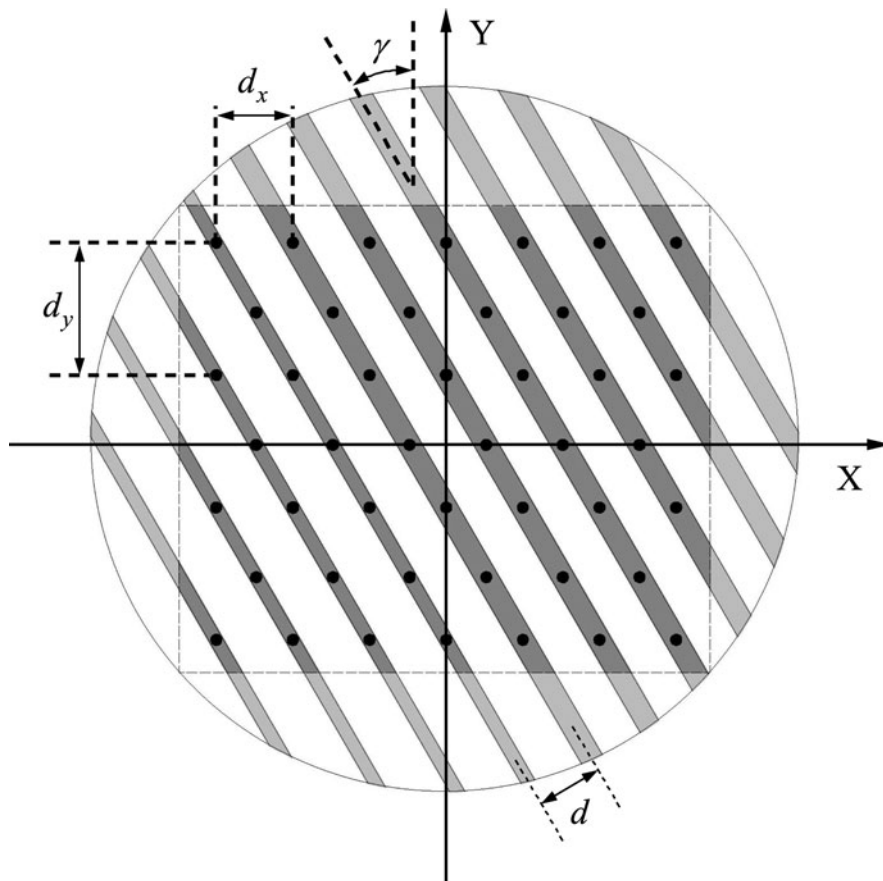**Fig. 3.** Schematic diagram of the equivalent array of VICTS when the plate is not rotating.

Fig. 4. Schematic diagram of the equivalent array of VICTS antenna when the plate rotates γ.
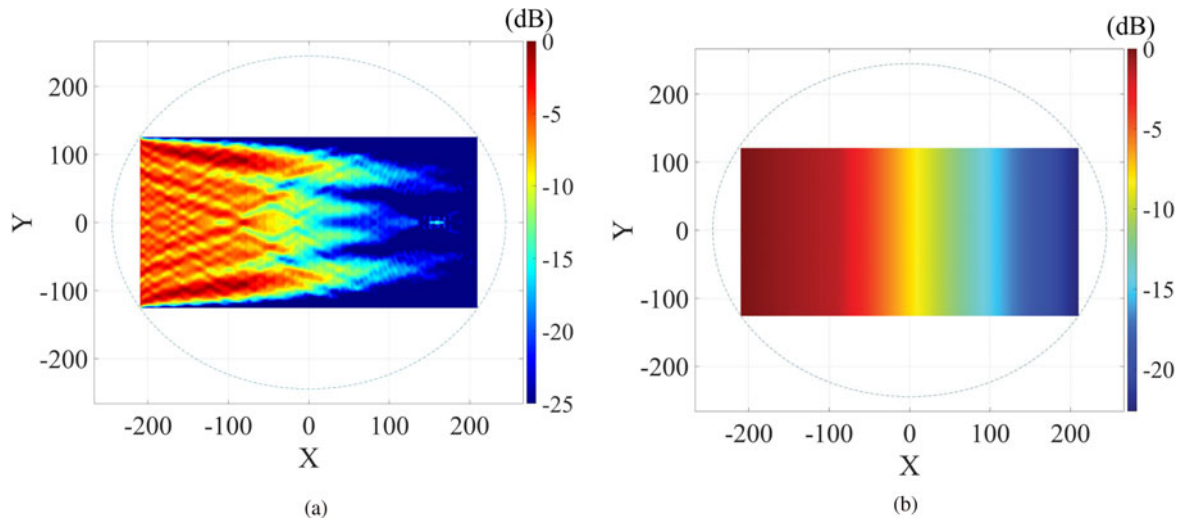
Fig. 5. Aperture field distribution of VICTS. (a) Results of full wave simulation, (b) Results of mathematical model calculation.
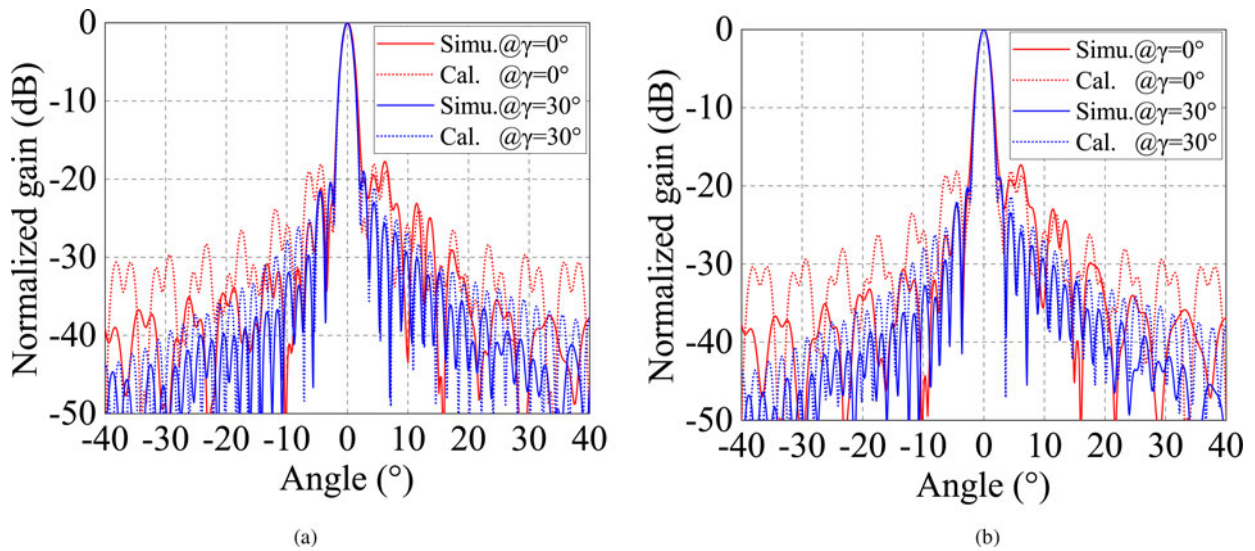

Fig. 6. Schematic diagram of the equivalent array of VICTS antenna when the plate rotates γ. (a) $h = 6$ mm (b) $h = 5$ mm.
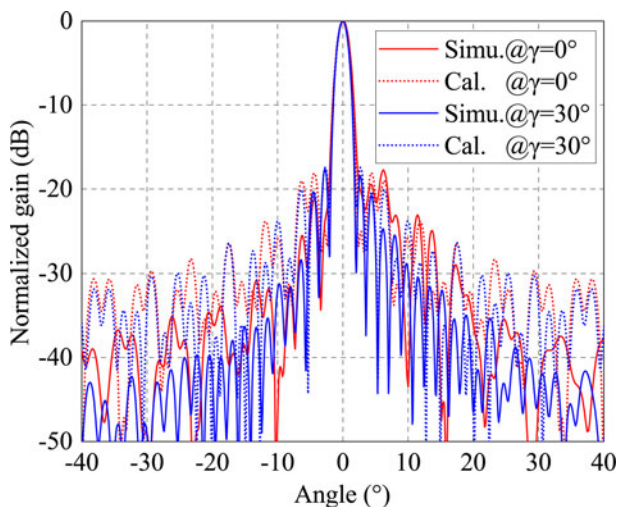

Fig. 7. Radiation pattern of VICTS antenna with three radiation branches.

plate is composed of a variety of branches with different radiation efficiency. After determining the position of each element and the number distribution of slots parallel to the X-axis, the electric field of each element can be expressed as:

$$\dot{I}_{mn} = \sqrt{\prod_{i=1}^{n} (1 - \eta_{i-1}) \, \eta_i} \, e^{j(k\varepsilon_e X_{mn})} \qquad \begin{aligned} m &= 1 \ldots M \\ n &= 1 \ldots N \end{aligned}$$

$$\eta_i = \begin{cases} 0, & i = 0 \\ \eta_{01}, & 0 < i \le N_0 \\ \eta_{02}, & N_0 < i \le N \end{cases} \tag{8}$$

Therefore, the pattern of the antenna can be expressed as:

$$F(\theta, \varphi) = \sum_{m=1}^{M} \sum_{n=1}^{N} C \dot{I}_{mn} e^{jk(X_{mn} \cos \varphi + Y_{mn} \sin \varphi) \sin \theta} \tag{9}$$
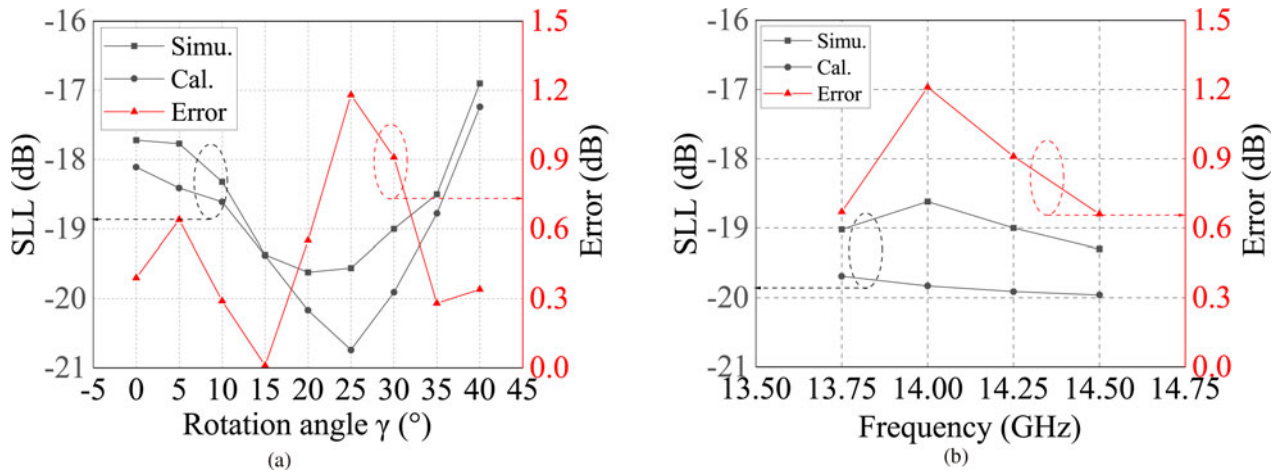
Fig. 8. SLL error in various cases. (a) f = 14.25 GHz (b) γ = 0°.
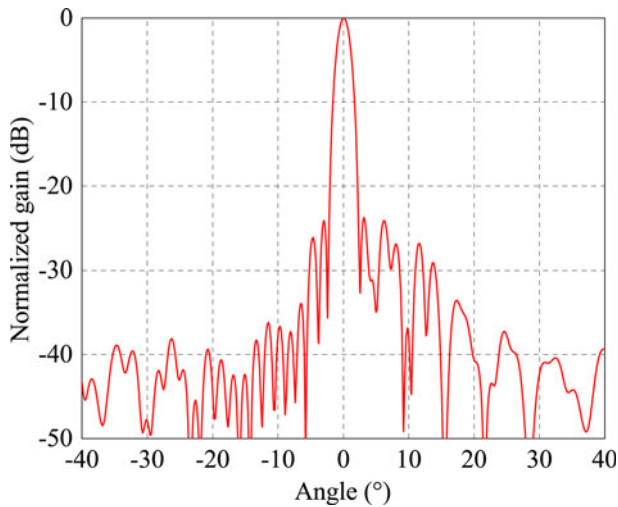

Fig. 9. Radiation pattern of VICTS antenna with low sidelobe design.

The antenna pattern is converted to $U - V$ coordinate by the following transformation:

$$u = \sin \theta \cos \varphi$$
$$v = \sin \theta \sin \varphi \qquad (10)$$

The short axis pattern of the antenna can be obtained by taking the section parallel to the U-axis and passing through the maximum value of the pattern.

Result analysis

In this section, the VICTS antenna with a radius of 350 mm working in 13.75–14.5 GHz band is used. Fig. 5(a) shows the simulation result of aperture field distribution of CST model, and Fig. 5(b) shows the aperture field distribution calculated by MATLAB. Because energy diffusion and energy reflection are not considered in the theoretical calculation model, the results of aperture field distribution of the theoretical calculation model are different from those of CST simulation model. However, the electric field along the X-axis has the same downward trend, so the theoretical calculation model can be used to estimate the SLL.

The simulation pattern and theoretical calculation pattern of the VICTS antenna in the short axis plane of 0° and 30° are shown in Fig. 6(a) when h is 6 mm. At different rotation angles, the waveforms of the two patterns are consistent. The position of sidelobe is calculated accurately, and the SLL error is less than 1 dB. Part of the reason for the SLL error is that the equivalent magnetic current is used as the antenna subarray to simplify the calculation. As shown in Fig. 6(b), when h is 5 mm, the SLL error is still consistent with Fig. 6(a). Therefore, it is feasible to replace subarray with equivalent magnetic current.

In order to verify that the model can be used in the case of more than two groups of different radiation branches, the simulation results and theoretical calculation results of the antenna model with three groups of radiation branches are given in Fig. 7. The patterns obtained by the two methods are still highly consistent. This model can be used to calculate the pattern of VICTS antenna with any group of different radiation branches.

Fig. 8(a) shows the SLL error at different angles. The plate rotation angle is from 0° to 50° and the pitch angle is from 5° to 70°, respectively. As can be seen from the figure, with the change of rotation angle γ, the SLL calculated by mathematical model and simulation results show the same variation trend, and the SLL error always remains below 1.2 dB under different rotation angles. When the antenna operates at different frequencies, the error between simulation and calculation remains at a low level (Fig. 8(b)). Therefore, the mathematical model can be used to calculate the SLL of the VICTS antenna and perform low sidelobe design.

Based on the mathematical model, the low sidelobe design of VICTS antenna is carried out by combining multiple radiation branches and nonlinear slow wave structure. The number of radiation branches and the height of slow wave structure at different positions are taken as optimization parameters. During the optimization process, the aperture field of the antenna evolved in a tapered distribution, so the SLL was reduced. The radiation pattern of the antenna is shown in Fig. 9, and the SLL reaches − 23.7 dB.

Conclusions

In this paper, a mathematical model for calculating the antenna pattern of VICTS is proposed. The mathematical model can accurately calculate the antenna pattern under different scanning angles and operating frequencies. The mathematical calculation results are consistent with the full-wave simulation results, and

the SLL error remains very low. The SLL of the VICTS antenna designed with this mathematical model can reach - 23.7 dB.

References

1. **Bayer H, Krauss A, Zaiczek T, Stephan R, Enge-Rosenblatt O and Hein MA** (2016) Ka-band user terminal antennas for satellite communications [antenna applications corner]. *IEEE Antennas and Propagation Magazine* **58**, 76–88.
2. **Ettorre M, Foglia Manzillo F, Casaletti M, Sauleau R, Le Coq L and Capet N** (2015) Continuous transverse stub array for Ka-band applications. *IEEE Transactions on Antennas and Propagation* **63**, 4792–4800.
3. **Pearson R** (April 2011) Next generation mobile SATCOM terminal antennas for a transformed world. in *Proc. Eur. Conf. Antennas Propag.*, Rome, Italy, pp. 2341–2345.
4. **Wan J, Lu S, Wang X and Ai Y** (2016) A steerable spot beam reflector antenna for geostationary satellites. *IEEE Antennas and Wireless Propagation Letters* **15**, 89–92.
5. **Washington G, Yoon H-S, Angelino M and Theunissen WH** (2002) Design, modeling, and optimization of mechanically reconfigurable aperture antennas. *IEEE Transactions on Antennas and Propagation* **50**, 628–637.
6. **Sandhu AI, Arnieri E, Amendola G, Boccia L, Meniconi E and Ziegler V** (2016) Radiating elements for shared aperture Tx/Rx phased arrays at K/Ka band. *IEEE Transactions on Antennas and Propagation* **64**, 2270–2282.
7. **Han G, Du B, Wu W and Yang B** (2015) A novel hybrid phased array antenna for satellite communication on-the-move in Ku-band. *IEEE Transactions on Antennas and Propagation* **63**, 1375–1383.
8. **Milroy WW, Coppedge SB and Lemons AC** (2005) Variable inclination continuous transverse stub array. U.S. Patent 6 919 854 B2, 7 19.
9. **Hao RS, Cheng YJ and Wu YF** (2020) Shared-aperture variable inclination continuous transverse stub antenna working at K- and Ka-bands for mobile satellite communication. *IEEE Transactions on Antennas and Propagation* **68**, 6656–6666.
10. **Milroy WW** (1991) The continuous transverse stub (CTS) array: basic theory, experiment, and application. *Proceedings of Antenna Applications Symposium, vol. 2*, pp. 253–283.
11. **Milroy WW** (1994) Continuous transverse stub element devices and methods of making same. U. S. Patent 5 361 076, November 1.
12. **Foglia Manzillo F, Ettorre M, Casaletti M, Capet N and Sauleau R** (2015) Active impedance of infinite parallel-fed continuous transverse stub arrays. *IEEE Transactions on Antennas and Propagation* **63**, 3291–3297.
13. **Tekkouk K, Hirokawa J, Sauleau R and Ando M** (2017) Wideband and large coverage continuous beam steering antenna in the 60-GHz band. *IEEE Transactions on Antennas and Propagation* **65**, 4418–4426.
14. **Lou T, Yang X-X, Qiu H, Yin Z and Gao S** (2019) Compact dualpolarized continuous transverse stub array with 2-D beam scanning. *IEEE Transactions on Antennas and Propagation* **67**, 3000–3010.
15. **Gao J, Lei X, Wu J and Li T** (2017) Theoretical model for patterns of VICTS antenna'. *2017 IEEE 17th International Conference on Communication Technology (ICCT)*, pp. 728–731.
16. **Lu X, Gu S, Wang X, Liu H and Lu W** (2017) Beam-scanning continuous transverse stub antenna fed by a ridged waveguide slot array. *IEEE Antennas and Wireless Propagation Letters* **16**, 16751678.
17. **You Y, Lu Y, Wang Y, Yang W, Hao Z, You Q and Huang J** (2019) High-performance E-Band continuous transverse stub array antenna with a 45° linear polarizer. *IEEE Antennas and Wireless Propagation Letters* **18**, 2189–2193.
18. **Potelon T, Ettorre M and Sauleau R** (2019) Long slot array fed by a non-uniform corporate feed network in PPW technology. *IEEE Transactions on Antennas and Propagation* **67**, 5436–5445.
19. **Porter BG** (2010) Closed form expression for antenna patterns of the variable inclination continuous transverse stub. *IEEE International Symposium on Phased Array Systems and Technology*, pp. 164–169.
20. **Potelon T, Ettorre M, Coq L, Bateman T, Francey J, Lelaidier D, Seguenot E and Sauleau R** (2017) A low-profile broadband 32-slot continuous transverse stub array for backhaul applications in *E*-band. *IEEE Transactions on Antennas and Propagation* **65**, 6307–6316.
21. **Verbitskii IL** (1980) Dispersion relations for comb-type slow-wave structures. *IEEE Transactions on Microwave Theory and Techniques* **28**, 48–50.
22. **You Y, Lu Y, You Q, Wang Y, Huang J and Lancaster MJ** (2018) Millimeter-wave high-gain frequency-scanned antenna based on waveguide continuous transverse stubs. *IEEE Transactions on Antennas and Propagation* **66**, 6370–6375.

Kexin wang received the BS degree from South China University of technology, Guangzhou, China, in 2019. And he is currently working at PLA Strategic Support Information Engineering University pursuing the MS degree. His main research interests include aperture antennas, high gain antennas, and beam steering antennas.
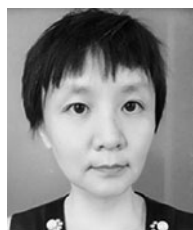

Xue Lei received the BS and MS degrees from PLA Strategic Support Information Engineering University, Zhengzhou, China, in 1989 and 2000, respectively. She is currently working at PLA Strategic Support Information Engineering University. Her main research interests include antenna and propagation.
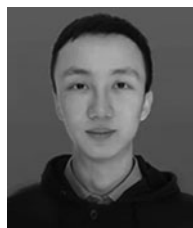
Jun Gao received the BS degree from PLA Strategic Support Information Engineering University, Zhengzhou, China, in 2015. His main research interests include aperture antennas, high gain antennas, and beam steering antennas.

Tianpeng Li received the BS and MS degrees from Air Force Engineering University, Xi'an, China, in 2012 and 2016, respectively. He is currently working at PLA Strategic Support Information Engineering University. Her main research interests include antenna and propagation.
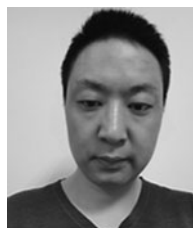
Mingyang Zhao obtained a bachelor's degree in electromagnetic field and microwave technology from the University of Information Engineering in 2013, and is currently studying for a Ph.D. in Information and Communication Engineering. His current research interests include phased arrays, antenna array synthesis, and optimization algorithms.